Title

Hydraulic and geomorphic processes in an overbank flood along a meandering, gravel-bed river: implications for chute formation

Journal

Earth Surface Processes and Landforms, 40(9)

ISSN

0197-9337

Authors

Harrison, Lee R
Dunne, Thomas
Fisher, G Burch

Publication Date

2015-07-01

DOI

10.1002/esp.3717

EARTH SURFACE PROCESSES AND LANDFORMS
Earth Surf. Process. Landforms (2015)

Published online in Wiley Online Library
(wileyonlinelibrary.com) DOI: 10.1002/esp.3717

Hydraulic and geomorphic processes in an overbank flood along a meandering, gravel-bed river: implications for chute formation

Lee R. Harrison,[1,2]* Thomas Dunne[3,4] and G. Burch Fisher[5]
[1] NOAA Fisheries, Santa Cruz, CA, USA
[2] Earth Research Institute, University of California-Santa Barbara, Santa Barbara, CA, USA
[3] Bren School of Environmental Science and Management, University of California-Santa Barbara, Santa Barbara, CA, USA
[4] Department of Earth Science, University of California-Santa Barbara, Santa Barbara, CA, USA
[5] Jackson School of Geosciences, University of Texas, Austin, TX, USA

Received 21 August 2014; Revised 2 February 2015; Accepted 4 February 2015

*Correspondence to: Lee R. Harrison, NOAA Fisheries, 110 Shaffer Rd, Santa Cruz, CA 95060, USA. E-mail: lee.harrison@noaa.gov

ESPL
Earth Surface Processes and Landforms

ABSTRACT: Hydraulic interactions between rivers and floodplains produce off-channel chutes, the presence of which influences the routing of water and sediment and thus the planform evolution of meandering rivers. Detailed studies of the hydrologic exchanges between channels and floodplains are usually conducted in laboratory facilities, and studies documenting chute development are generally limited to qualitative observations. In this study, we use a reconstructed, gravel-bedded, meandering river as a field laboratory for studying these mechanisms at a realistic scale. Using an integrated field and modeling approach, we quantified the flow exchanges between the river channel and its floodplain during an overbank flood, and identified locations where flow had the capacity to erode floodplain chutes. Hydraulic measurements and modeling indicated high rates of flow exchange between the channel and floodplain, with flow rapidly decelerating as water was decanted from the channel onto the floodplain due to the frictional drag provided by substrate and vegetation. Peak shear stresses were greatest downstream of the maxima in bend curvature, along the concave bank, where terrestrial LiDAR scans indicate initial floodplain chute formation. A second chute has developed across the convex bank of a meander bend, in a location where sediment accretion, point bar development and plant colonization have created divergent flow paths between the main channel and floodplain. In both cases, the off-channel chutes are evolving slowly during infrequent floods due to the coarse nature of the floodplain, though rapid chute formation would be more likely in finer-grained floodplains. The controls on chute formation at these locations include the flood magnitude, river curvature, floodplain gradient, erodibility of the floodplain sediment, and the flow resistance provided by riparian vegetation. Copyright © 2015 John Wiley & Sons, Ltd.

KEYWORDS: meandering river; floodplain; chute cutoff; flow resistance; riparian vegetation

Introduction

As water is decanted from river channels to adjacent floodplains during overbank discharge, the flow interacts with the floodplain topography and vegetation, leading to the development of off-channel chutes under favorable circumstances (McGowen and Garner, 1970; Constantine *et al.*, 2010; Grenfell *et al.*, 2012). The locations at which flow leaves the channel with a capacity to erode chutes are influenced by the in-channel flow field and by riparian vegetation. Chute channels develop on floodplains where water leaves the channel with sufficient depth and velocity and retains enough momentum, despite the drag of the floodplain vegetation and surface, to scour floodplain sediment, and also has sufficiently low sediment load to allow scour and to avoid sedimentation in any pre-existing depression. Gaining a better understanding of the processes that lead to chute formation requires an examination of the flow field as water interacts with the river channel, and with the floodplain topography and vegetation. Detailed studies of the exchange of flow between channels and the floodplain are usually conducted in laboratory facilities (Wormleaton *et al.*, 2004), and studies documenting the erosion of the chutes themselves are generally limited to qualitative observations (Tal and Paola, 2007; Braudrick *et al.*, 2009).

In the field, chute channels have been observed to develop in two types of locations along single-thread sinuous channels: immediately downstream of the bend apex, and across point bars. We are ignoring the case where flow obstructions such as ice jams and log jams lower the water level and allow headward erosion of a gully across the point bar (Gay *et al.*, 1998). The first case was interpreted in qualitative terms by McGowen and Garner (1970) from field observations along coarse sand-fine gravel bed rivers in Texas and Louisiana. The interpretation was that chutes develop on convex sides of streams during extreme floods when the thread of maximum velocity shifts from the concave toward the convex bank and

extends over the upstream part of the convex bank, scouring a channel through which bedload is transported in the extreme floods. At the same time, the inward shifting of the thread of maximum velocity intensifies accretion of sediment onto the point bar.

Constantine *et al*. (2010) associated chute formation with the progressive formation of embayments incised into the channel bank immediately downstream of the apex of a bend in a zone where their two-dimensional (2D) flow modeling identified the locus of fast overbank flow. At this location, in-channel velocities are high because of the interaction of the downstream pressure-gradient force, centrifugal force related to the bend, and the increase in cross-channel momentum transfer because of the geometry of the point bar. The upper part of this high-velocity flow is then expelled from the channel where the bank diverges most rapidly from its downstream direction (Wormleaton *et al*., 2004, figure 23). Water exiting the channel at or beyond the bend apex enters the floodplain at the rate of the outer bank velocity and slows at a rate that depends on the floodplain topography and flow resistance (Constantine *et al*., 2010). The development of floodplain chutes is sensitive to the density of floodplain vegetation, with relatively rigid, thin and dense woody vegetation providing resistance to floodplain incision (Smith, 2004).

More recent studies have identified a chute cutoff mechanism that involves channel incision across the point bar, either cutting an entirely new channel or occupying a swale between scroll bars. Grenfell *et al*. (2012) showed that these chutes formed between the point bar and floodplain when outer bank migration rates exceeded rates of bar growth in large sand-bedded rivers on three tropical floodplains. Chute initiation was favored by high rates of bend extension perpendicular to the valley axis, and the majority of them formed during scroll-slough development. Rapid extension favored chute initiation by breaking the continuity of point bar deposition and vegetation encroachment, resulting in widely-spaced scrolls with intervening sloughs that become progressively aligned with the down-valley floodplain flow as the bend itself extends normal to the down-valley direction. Since these pathways are straighter and steeper than the original channel, they also have a gradient advantage. Progressive occupation and widening of scroll-sloughs were also documented by Mertes *et al*. (1996) on the Amazon River, but not investigated as thoroughly as the work of Grenfell *et al*. (2012). Dunne and Aalto (2013) suggested that such chutes would also be favored by low suspended sediment concentrations, low accretion rates of point bar sediment that allow higher rates of flow across the point bar and leave swales open for long periods of time, and sustained overbank flows. Chutes may also form across the bar surface when deposition of coarse sediment is not located at the bar–floodplain transition but closer to the channel centerline, as observed in the laboratory experiments of Braudrick *et al*. (2009). Such chutes can initiate the transformation from single to multi-threaded channels, as central bar deposits cause water divergence into more than one active channel, as demonstrated by the experimental work of Bertoldi and Tubino (2005).

Processes of chute formation are usually triggered by floods, as bar development and chute cutoff require high water levels and high bed material transport potential. Due to the difficulties in collecting hydraulic data during high flows, very few field data exist documenting the hydraulic interactions between meandering channels and floodplains during overbank floods. Laboratory flumes (Sellin *et al*., 1993; Wormleaton, 1996; Shiono and Muto, 1998) and numerical modeling (Nicholas and McLelland, 2004) have been used much more widely to study channel–floodplain interactions. The processes of flow exchange between sinuous channels and floodplains were studied in a compound laboratory flume by Sellin *et al*. (1993), Knight and Shiono (1996), and Wormleaton *et al*. (2004). The channel had a sinuosity of 1.4, a meander wavelength of 12 m, a width/depth ratio of 0.15 m and a floodplain flow depth of 0.05 m. The floodplain surface was smoothed concrete and had a gradient of 0.001. Tracing and modeling of the flow illustrated that peak velocities and boundary shear stresses occur downstream from the maxima in bend curvature, and that flow exiting the channel over the concave bank at that location applied a high shear stress to the bank. Sellin *et al*. (1993) and Wormleaton *et al*. (2004) also illustrated that overbank flow from the floodplain entering the straight section between bends would roll over the in-channel water and initiate a helical motion that grew until the next bend, cancelling and even reversing helical motion to be expected from the centrifugal force associated with the channel curvature. This conception of channel–floodplain flow interactions was adopted by Morvan *et al*. (2002) who argued for the necessity of three-dimensional (3D) computational fluid dynamics (CFD) models to represent the highly 3D nature of the velocity field in meandering compound channels with overbank flow. However, Wormleaton *et al*. (2004) also commented that the flow reversal was observed only when the flow from the floodplain was deep and fast, and it did not occur when that flow entering the straight section was shallower and slower, as might occur with rougher floodplains. Little progress has yet been made in testing how the insights gained from laboratory studies of overbank flows translate to the field, and how well existing hydrodynamic models predict channel–floodplain flow interactions and the initiation and location of chute channels.

Motivation

The purpose of our study was to illustrate how flow within the channel and on the floodplain create conditions for chute formation. Thus, our first task was to document the interactions between flows in a meandering channel and its thinly vegetated, topographically smooth (recently re-constructed) floodplain during an overbank flow. The second task was to compare numerical predictions of flow and shear stress, confirmed by the field measurements, with the locations of surveyed chute channel initiation. The organization of the flow field both within the channel and on the floodplain surface affects the intensity and location of the chute-forming discharges of erosive water from the channel. The research was organized by the following questions:

1. What is the nature of the in-channel flow field in curved reaches of a meandering river during an overbank flood?
2. How is water conveyed overbank onto a sparsely vegetated floodplain?
3. How concentrated is the erosive potential as water is decanted onto the floodplain and decelerated by the vegetated substrate?
4. Where and under what circumstances is water expelled onto the floodplain competent to erode chute channels?

Outline of Study and Site Characteristics

We characterized the flow field in a meandering channel and floodplain using an integrated field and modeling approach, involving detailed surveys of the river channel and floodplain topography and opportunistic velocity measurements, collected in the channel and floodplain during an overbank flood. We

measured the height and areal extent of floodplain vegetation in order to develop a spatially explicit representation of the floodplain flow resistance for use in a 2D flow model. We then calibrated and validated the hydrodynamic model in order to expand the interpretation of the field measurements. The velocity measurements provided a means to quantify the 3D nature of the flow field in the channel, as well as the rate of deceleration as water spills onto the floodplain. We used the velocity measurements to verify the flow model predictions, which has not been widely done at the field scale in previous overbank modeling studies (see Nicholas and McLelland, 2004; Stoesser *et al.*, 2003 for notable exceptions).

The study was conducted in a reach of the Merced River, California (latitude 37°29′N, longitude 120°28′W), reconstructed in 2002, which consists of a single-threaded, meandering river and sparsely vegetated floodplain surface (Figure 1). The channel and floodplain were re-constructed after a peak flow of 234 m^3 s^{-1} (approximately a 50 year flood based on a log Pearson type III analysis calculated from the post-dam annual peak flow data for 1967 to 2012) caused the channel to avulse into a floodplain gravel mining pit, and transition from a single-threaded to a multi-threaded channel (CADWR, 2005). The re-engineered reach has a gravel bed (D_{50} = 57 mm) and the bank material is composed of loose, unconsolidated gravel and cobble (Harrison *et al.*, 2011; Table I provides additional site characteristics). The floodplain was designed as a nearly planar surface with the same grain-size composition as the river channel bed, each with a sand content of ~5%. Floodplain width varies from 250 to 500 m, ~9–17 times the bankfull channel width of 29 m. In the decade since construction, willow and cottonwood trees have colonized the channel margins and point bars, while most of the floodplain is covered with sparse shrubs, grasses and exposed gravel.

Table I. Physical characteristics of the study site on the Merced River, California

Bed gradient	0.0025
Floodplain gradient	0.003
Bankfull discharge (m^3 s^{-1})	42.5
Channel width (m)	29.0
Mean bankfull depth (m)	1.00
D_{16} (mm)	32
D_{50} (mm)	57
D_{84} (mm)	95
Sinuosity	1.16
Meander wavelength (m)	523
Bend apex radius of curvature (m)	95–133

Chutes have begun to form in two locations along this reconstructed reach of the Merced River: immediately downstream of a bend apex, as suggested by Constantine *et al.* (2010) and across the point bar along a developing scroll-slough, as observed by Mertes *et al.* (1996), Braudrick *et al.* (2009), and Grenfell *et al.* (2012). The rate of evolution of these emerging chutes has been slow because the texture of the floodplain surface in the reach is coarse. However, their locations and

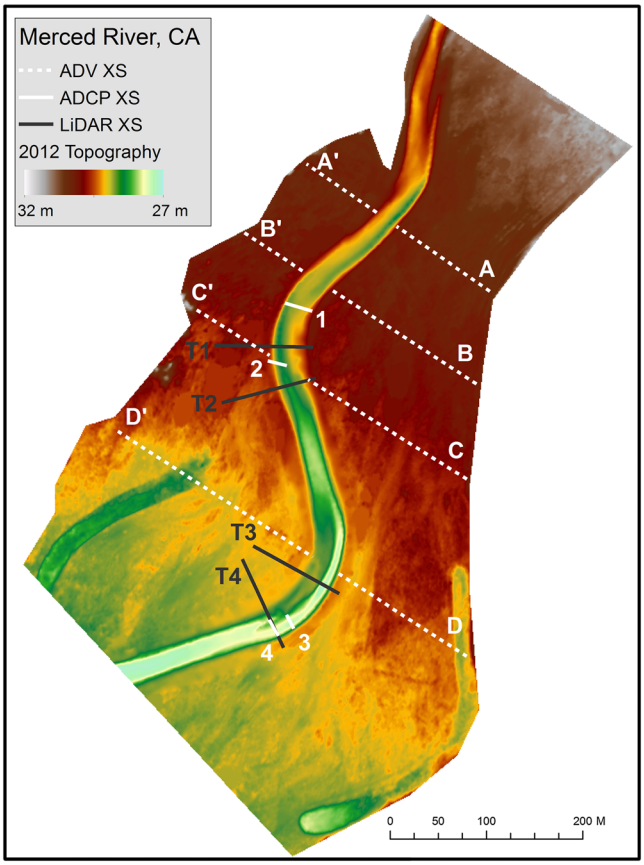

Figure 1. River channel–floodplain topography of the study reach of the Merced River. Also shown are the locations of the velocity transects (1–4 for the channel and A–D for the floodplain) collected during the five-year overbank flood and topographic profiles (T1–T4) documenting the location of developing floodplain chutes. The direction of flow is from the top of the image to the bottom. Two engineered floodplain channels occur at the floodplain margins, intersected by transect D–D′, are not connected to the reconstructed channel. Computational experiments with these floodplain channels filled and unfilled with sediment indicated no differences in the modeled channel–floodplain exchanges or predictions of chute incision. This figure is available in colour online at wileyonlinelibrary.com/journal/espl

relationships to the hydrodynamics of channel–floodplain flow reflect general mechanisms applicable to chutes that evolve more rapidly where the floodplain surface is much finer and flow confinement can be established more abruptly.

Flow in the reach is regulated by upstream dams, and an unusually deep snow pack in 2011 required sustained flow releases to increase reservoir storage. These reservoir releases resulted in 129 days of overbank flow with a peak discharge of 140 $m^3\ s^{-1}$, which is 3.3 times the bankfull discharge of 42.5 $m^3\ s^{-1}$ and has a recurrence interval of 5.8 years determined from a log Pearson type III analysis calculated from the post-dam annual peak flow data (1967–2012).

Methods

Topographic and vegetation surveys

The river channel topography was surveyed with real-time kinematic (RTK) global positioning system (GPS) receivers with a vertical accuracy of 0.01 m. Elevations were measured along transects with an average streamwise spacing of 7 m and an average cross-stream point spacing of 2 to 3 m. Extra points were surveyed along breaks in slope, such as the top and base of the bank, and in areas of more complex topography. The raw data were interpolated to form a continuous topographic surface using a specialized kriging method for curved channels developed by Legleiter and Kyriakidis (2008). The floodplain topography and vegetation were measured by means of terrestrial LiDAR (light detection and ranging) scans (TLS) using a Riegl LMS-Z420i (Perroy *et al.*, 2010). The resulting points were filtered to classify both ground and vegetation heights at a gridded spatial resolution of 0.5 m.

Hydraulic data

Two sets of hydraulic data were collected during a flood discharge of 106.5 $m^3\ s^{-1}$ (2.5 × the bankfull discharge) to characterize the flow fields in the channel and floodplain. In-channel velocity fields were measured at two bends shown in Figure 1 with a SonTek S5 acoustic Doppler current profiler (ADCP), equipped with an integrated, sub-meter accuracy differential GPS. The ADCP has five transducers, with four beams angled at 25° operating at 3.0 MHz and a single vertical beam echosounder which samples at 1.0 MHz. We attached the ADCP to a moving boat and two passes were made along each of four transects to measure the streamwise (u), cross-stream (v) and vertical (w) velocities in the channel and along the outer channel banks. The ADCP measured velocity profiles in 0.1 m vertical increments, but its sensor depth (0.1 m) and blanking distance (0.2 m) limited reliable velocity data along the shallow margins where flow depths were less than 0.3 m. The Velocity Mapping Toolbox (VMT) (Parsons *et al.*, 2013) was used to project repeated ADCP transects onto a uniform grid, using a horizontal and vertical grid node spacing of 1 m and 0.1 m, to rotate individual velocity ensembles to ensure zero net secondary discharge in the lateral plane (Markham and Thorne, 1992), to calculate primary and secondary velocities (Lane *et al.*, 2000) and to smooth velocity ensembles using a nearest neighbor approach. In areas where the ADCP did not measure reliable near-bed velocities (the lower 10% of flow depth), a logarithmic profile was fitted to the measured part of the flow field and projected from the lowermost valid velocity measurement to zero velocity at the bed, using a Nikuradse roughness length of $z_o = D_{50}/30$.

Three-dimensional velocity measurements on the inundated floodplain were made with a Sontek acoustic Doppler velocimeter (ADV) at eight transects shown in Figure 1. The ADV was positioned perpendicular to the visually estimated down-valley direction with the sensor at 40% of the flow depth above the bed and deployed for a period of 60 seconds at a sampling frequency of 1 Hz.

Flow modeling

The goal of the flow modeling was to characterize the flow velocity and boundary shear stress on the channel bed, banks and floodplain to extend our interpretations beyond the limited extent of the field measurements. We applied the Multidimensional Surface Water Modeling System (MD-SWMS) interface for the Flow and Sediment Transport Morphological Evolution of Channels (FaSTMECH) model developed by the US Geological Survey (Lisle *et al.*, 2000; Nelson *et al.*, 2003; Barton *et al.*, 2005). FaSTMECH solves the depth-averaged form of the Navier–Stokes equations, expressed in a channel-centered, orthogonal coordinate system (Nelson *et al.*, 2003; McDonald *et al.*, 2005). Complete details of the model can be found in Nelson *et al.* (2003). The model grid was 800 m long by 675 m wide and covered the entire floodplain, with a spacing of 2.0 m in the streamwise and cross-stream directions. This grid node spacing was established in a model of overbank flow in the same reach, described by Harrison *et al.* (2011). While more complex 3D hydrodynamic models exist, depth-averaged flow models have been applied successfully to investigate overbank flows in natural channels and floodplains (Nicholas and Mitchell, 2003) and remain widely used tools in studies of river and floodplain morphodynamics (Crosato and Saleh, 2011; Li and Millar, 2011; Nicholas, 2013).

The hydraulic model boundary conditions included a specified total discharge at the upstream boundary and a downstream water surface elevation. The flow into the model reach is confined to the upstream channel and floodplain, which is of similar width and gradient and does not have any lateral inflows. This allowed us to specify a single inlet over which the discharge entered the model reach. Initial conditions for the model were specified by performing one-dimensional hydraulic calculations, based on the known discharge, downstream stage, and calibrated drag coefficient (see later), to determine a water surface elevation at the upstream end of the computational domain. Numerical experiments were conducted in which we partitioned the velocity distribution at the inlet such that 50% of the discharge entered the channel, while the other 50% entered the model reach over the floodplain. This estimated velocity distribution was based on our hydraulic measurements collected in the channel and floodplain during the overbank flood observed. Results from these modeling experiments determined that the hydraulic measurement data used for calibration and validation were insensitive to the specified upstream velocity distribution, as the field data were collected at a sufficient distance downstream from the entrance to the modeled reach. Therefore, we did not specify an upstream model velocity distribution and allowed the model to determine how the flow was distributed across the inlet. The downstream water surface elevation was obtained through direct measurements of the flood stage using a total station.

Flow resistance and boundary shear stress

The effects of friction due to sediment grains and vegetation were modeled through the flow resistance term in the shallow

water equations solved by FaSTMECH. In model grid cells where only sediment grains were present (i.e. no vegetation), the grain friction was represented using spatially explicit drag coefficients, c_d, which were calculated as a function of the local flow depth and sediment grain-size following McDonald *et al*. (2005):

$$c_d = \left[\left(ln\left(\frac{h}{z_0}\right) - 1\right)/k\right]^{-2} \quad (1)$$

where h is the flow depth (in meters), z_o (in meters) is the roughness length = (D_{50}/30) and k is von Karman's constant (≈0.408). Values of c_d were calculated by first running FaSTMECH with a uniform c_d = 0.02 (Harrison *et al*., 2011), to compute a first approximation of the flow depth, h, at each node in the computational grid. Spatially explicit values of c_d were then calculated for the channel and unvegetated floodplain using Equation (1), with the assumption that the grain-size was spatially uniform for both the channel and floodplain (D_{50} = 57 mm).

Vegetation increases the local flow resistance and decreases the velocity, thus on vegetated floodplains some means of including the drag effect of plants on the flow field is essential for accurate hydrodynamic predictions. The plant height, stem diameter and density will vary spatially across the floodplain, in accordance to the plant age, soil moisture and other environmental factors. Nevertheless, it is commonly accepted that the effects of emergent vegetation on the flow field can be represented in numerical models as a set of evenly spaced cylinders with constant density and stem diameter (see Vargas-Luna *et al*., 2014 for a comprehensive review).

In areas of the channel margins and floodplain where vegetation was present, we approximated the effect of trees and shrubs on the flow velocity using a drag force approach, where the drag coefficient term for vegetation, c_{dv}, was defined as:

$$c_{dv} = \frac{1}{2} C_D \alpha \quad (2)$$

where c_d is the drag coefficient of a woody stem and α is a vegetation density parameter. We selected a c_d of 1.2 for individual plant stems, based upon drag coefficients for rigid cylinders at high Reynolds numbers (Kean and Smith, 2004). The vegetation density term α, was defined after Takebayashi and Okabe (2009) as:

$$\alpha = \frac{n_s D_s h_v}{s^2} \quad (3)$$

where n_s is the number of plant stems per model grid cell, D_s is the average stem diameter (in meters), h_v is the submerged depth of vegetation in meters (assumed to be the water depth in the case of emergent vegetation) and s^2 is the model grid cell area (in m^2). The vegetation density term α, represents the proportion of the cross-sectional area of each cell that is occupied by vegetation. Values of D_s (0.2 m) for individual trees were estimated from field data on the Merced River (O. Soong, 2012 unpublished data), while the vegetation height, h_v, was calculated by taking the difference between the highest and lowest TLS points in a given 0.5 m cell. The values of h_v represent a maximum vegetation height, and because we could only specify a single vegetation height per model grid cell we did not include shorter grasses. Therefore it is possible that we underestimated the flow resistance in those cells that contained both trees and grasses. For areas of the floodplain completely covered by grass, c_{dv} was set equal to 0.05, based on the laboratory experiments of Wilson and Horritt (2002).

The general approach for representing the effects of vegetation on the flow resistance has been widely used (see Corenblit *et al*., 2007 for review) and is similar to previous studies where energy losses due to vegetation have been expressed in terms of Manning's n (Fathi-Maghadam and Kouwen, 1997) or the Chezy C (Baptist, 2005). In this study, including the additional effects of plant stem flexibility and added flow resistance due to leaves (Nepf, 2012) was deemed unnecessary, as we observed minimal plant stem bending of the partially submerged riparian trees during the overbank flood of interest and there were very few leaves on the trees at the time of the flood. While the simple drag force approach used here does not provide information on some of the local complexities that arise as water flows through and around emergent vegetation, it was considered suitable for investigating the potential for floodplain chute formation.

In the shallow water equations solved by FaSTMECH, the boundary shear stress (τ_b) is expressed as:

$$\tau_b = \rho c_{dt} \langle U \rangle^2 \quad (4)$$

where ρ is the fluid density (in kg m^{-3}), c_{dt} is the total drag coefficient due to grain friction and vegetation ($c_{dt} = c_d + c_{dv}$), $\langle U \rangle$ is the velocity magnitude calculated by FaSTMECH and $\langle\rangle$ denotes vertically-averaged quantities. For the purpose of assessing sediment mobility, we first calculated the depth-averaged velocity using FaSTMECH and a total drag coefficient which accounts for the effects of friction due to both sediment and vegetation. We then calculated the bed shear stress due to grain friction (τ_g), using the modeled values of $\langle U \rangle$ and by replacing c_{dt} with c_d in Equation (4). To assess the potential for sediment mobility of bare sediment, we calculated a dimensionless Shields stress:

$$\tau^*_{50} \equiv \frac{\tau_g}{(\rho_s - \rho) g D_{50}} \quad (5)$$

where ρ_s is the density of sediment (in kg m^{-3}), g is acceleration due to gravity (m s^{-2}) and D_{50} (in meters) is the median particle diameter. Sediment was assumed to be mobile at τ^*_{50} values equal to or greater than 0.03 after Buffington and Montgomery (1997). We recognize that sediment mobility varies with particle sorting (Wiberg and Smith, 1987) and gradient (Lamb *et al*., 2008), and τ^*_{50} has been measured to be 0.021 at the study site (Wydzga *et al*., 2007), but we selected a single, widely-employed value for the purposes of simplification.

Model simulations

The model was calibrated by adjusting the flow resistance due to sediment grains (c_d) and vegetation (c_{dv}) to optimize the fit between measured and predicted water depths. The first step in the model calibration involved adjusting the spatially explicit values of the skin drag coefficient, c_d, for the channel. The calibration was performed by running the model for the observed discharge (Q = 106.5 m^3 s^{-1}) and adjusting c_d to minimize the root mean square error (RMSE) between measured water depths, collected with the ADCP and modeled depths.

Values of c_d were then set in the channel for the remainder of the model runs, while the floodplain was assigned values of $c_d + c_{dv}$. In model grid cells where floodplain vegetation was present, values of the vegetation drag coefficient, c_{dv}, were calibrated by holding the values of c_d (1.2) and d_s (0.2 m) constant and adjusting the value of n_s to minimize the RMSE between measured floodplain depths collected with the ADV and predicted depths. A value of $n_s = 4$ was found to provide the best fit between measured and modeled depths and was adopted for all remaining model runs.

The calibrated flow model was used to simulate the hydrodynamics of the observed five-year flood in order to test the model's predictive capability and to help expand our interpretation beyond the sparse field data. A second set of model calculations was used to investigate the channel–floodplain hydraulics over a broader range of flows, from bank full discharge up to a 100-year flood. The downstream stage–discharge relation required for the unmeasured flows was developed using a HEC-RAS model, calibrated to measured water surface elevations collected during a discharge equal to 120.5 $m^3\ s^{-1}$ in March 2005 (reported in Harrison *et al.*, 2011) with a RMSE = 0.15 m.

Results

Measured flow fields

Figure 2 shows secondary circulation (*v*, *w*) vectors and shaded values of the velocity magnitude (*U*) in the four ADCP cross-sections labeled in Figure 1. Peak values of *U* were located near the channel centerline upstream of the bend apex (Figure 2A) and shifted towards the deepest part of the pool downstream from the bend apex (Figures 2C and 2D). Secondary circulation was observed in the meander bends at each of the four ADCP transects, with a strong outward directed velocity near the surface and inward directed velocity near the river bed, resulting in helical flow cells consistent with secondary flow patterns observed in meandering rivers during in-bank flows (Figure 2). Inward directed flow was observed in the deepest portion of each pool, and tended to weaken as flow was swept up the pool towards the bar, where near-bed cross-stream velocities (*v*) diminished to essentially zero (Figure 2A) or were oriented completely toward the outer bank over the point bar (Figure 2C). Measured vertical velocities (*w*) were small in comparison to the *u* and *v* components, comprising 3% of the total velocity

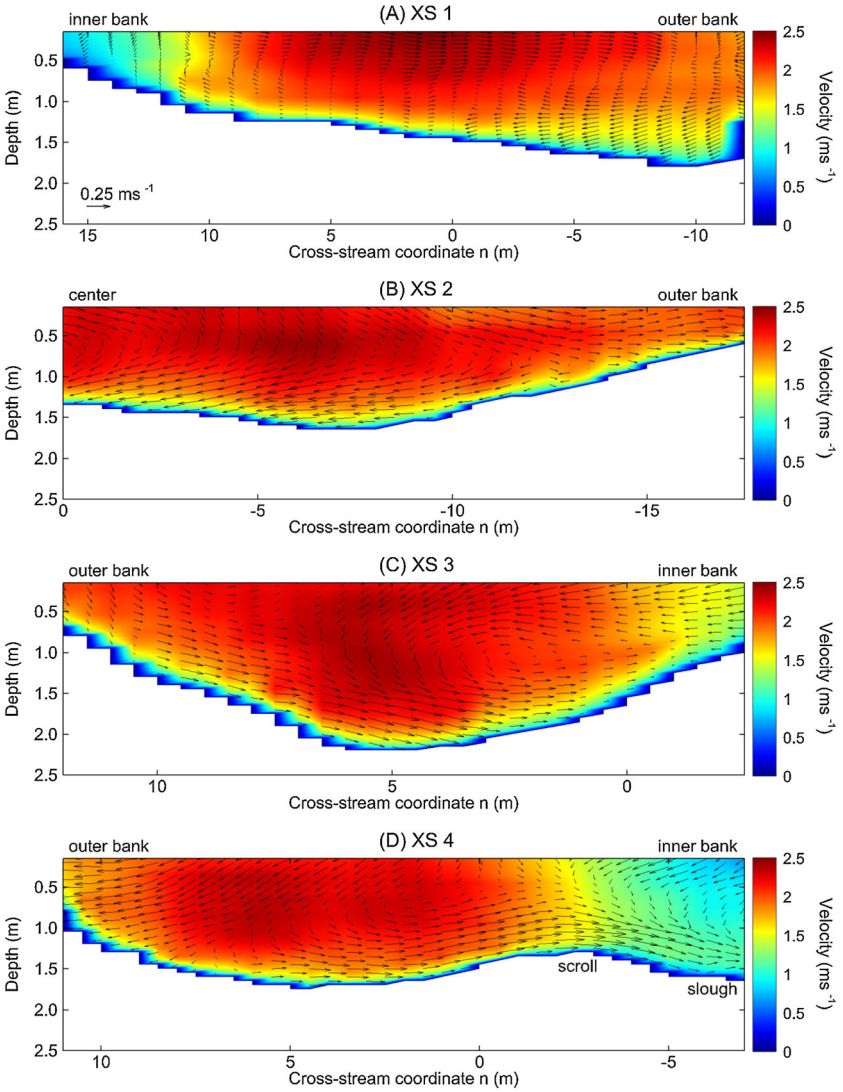

Figure 2. Three-dimensional velocity data collected with an ADCP during a five-year flood, showing the secondary circulation (*v*, *w*) vectors and shaded values of the velocity magnitude (*U*). View is downstream and the cross-stream coordinate *n* is referenced to the centerline (*n* = 0), with larger negative (positive) values toward the right (left) bank. Due to difficulty in navigating the jet boat near the shallow banks, we were not able to measure portions of the point bars or the top of the river bank with the ADCP, thus our transects did not span the entire 29 m bankfull channel. This figure is available in colour online at wileyonlinelibrary.com/journal/espl

magnitude (U). We did not observe a secondary outer bank helical flow cell of opposite rotation, consistent with previous laboratory studies conducted in curved flumes where the counter-rotating circulation cell only develops along the outer bank in channels where the width/depth ratio < 10 (Blanckaert and Graf, 2001; Termini and Piraino, 2011).

The mean value of measured $\langle U \rangle$ was 0.4 m s^{-1} for the floodplain and 1.6 m s^{-1} for the channel. Mean floodplain flow depth for the four transects was 0.3 m and the average flow depth over the measured channel cross-sections was 1.4 m. The transfer of water from the channel to the floodplain was estimated at a single bend using the channel and floodplain velocity data. Using the outermost depth-averaged velocity, $\langle U \rangle$, measurement from ADCP transect 1, we determined that water was advected from the channel to the floodplain at a rate of 1.7 m s^{-1} and decelerated by approximately 50% after traveling 50 m onto the downstream floodplain, where we measured $\langle U \rangle$ = 0.9 m s^{-1} with the nearest ADV cross-section. The flow depth (h) equaled 1.3 m at the outermost ADCP measurement and 0.4 m on the floodplain where the ADV measurement was made.

Flow model calibration and validation

Figure 3 compares the measured and predicted flow depths and velocities for the channel and floodplain; the RMSE between the observed and predicted depths was 0.13 m and 0.08 m for the channel and floodplain respectively, while the RMSE between the measured and predicted velocities was 0.2 m s^{-1} for the channel and 0.18 m s^{-1} for the floodplain. Results from a regression analysis comparing the measured and predicted vertically-averaged, streamwise $\langle u \rangle$, cross-stream $\langle v \rangle$ and velocity magnitude $\langle U \rangle$ are summarized in Table II.

There was good overall agreement between the cross-stream variation in measured and predicted velocities (Figures 4 and 5), with an increased discrepancy between observed and predicted floodplain velocities with distance from the channel margins (Figure 5). This disagreement may be due to small-scale topographic features that were smoothed out on the interpolated floodplain surface that was generated using the 2 m × 2 m computational grid. Nevertheless, the modeled velocities tend to follow a similar rate of decline from the channel margin across the width of the floodplain (Figure 5). FaSTMECH was able to predict the flow deceleration that occurred as water left the channel and traveled across the floodplain, as confirmed by the close agreement between the measured (1.7 m s^{-1}) and predicted (1.55 m s^{-1}) outerbank channel velocity at ADCP XS 1 (Figure 4), and the measured (0.9 m s^{-1}) and predicted (0.8 m s^{-1}) floodplain velocities at ADV transect C′ (Figure 5).

Table II. Results from regression analyses comparing measured and predicted vertically-averaged, streamwise $\langle u \rangle$, cross-stream $\langle v \rangle$ and velocity magnitudes $\langle U \rangle$

Velocity component	Q (m^3 s^{-1})	b_1	b_0	R^2	RMSE (m s^{-1})
Streamwise velocity component $\langle u \rangle$	106.5	0.78	−0.08	0.92	0.19
Cross-stream velocity component $\langle v \rangle$	106.5	0.96	−0.05	0.89	0.21
Velocity magnitude $\langle U \rangle$	106.5	0.97	0.04	0.94	0.19

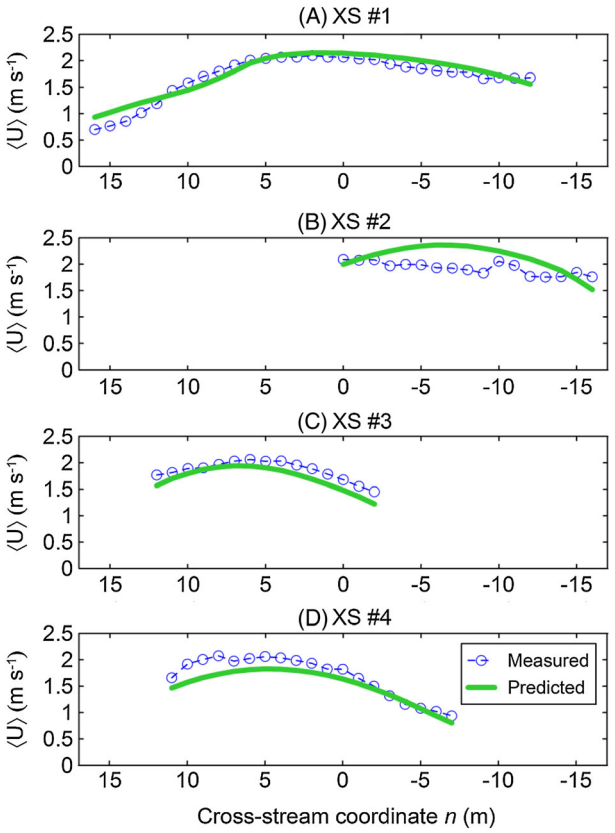

Figure 4. Comparison between measured channel depth-averaged velocity magnitudes with those predicted by FaSTMECH. This figure is available in colour online at wileyonlinelibrary.com/journal/espl

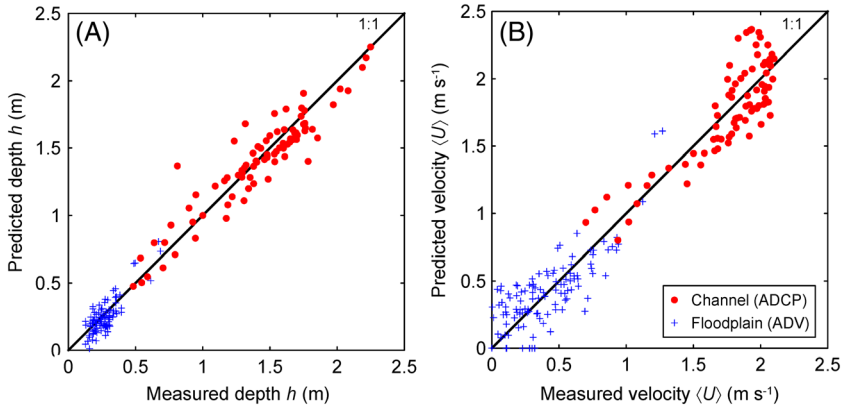

Figure 3. Comparison between measured and predicted (A) flow depths and (B) depth-averaged velocities in the channel and on the floodplain. This figure is available in colour online at wileyonlinelibrary.com/journal/espl

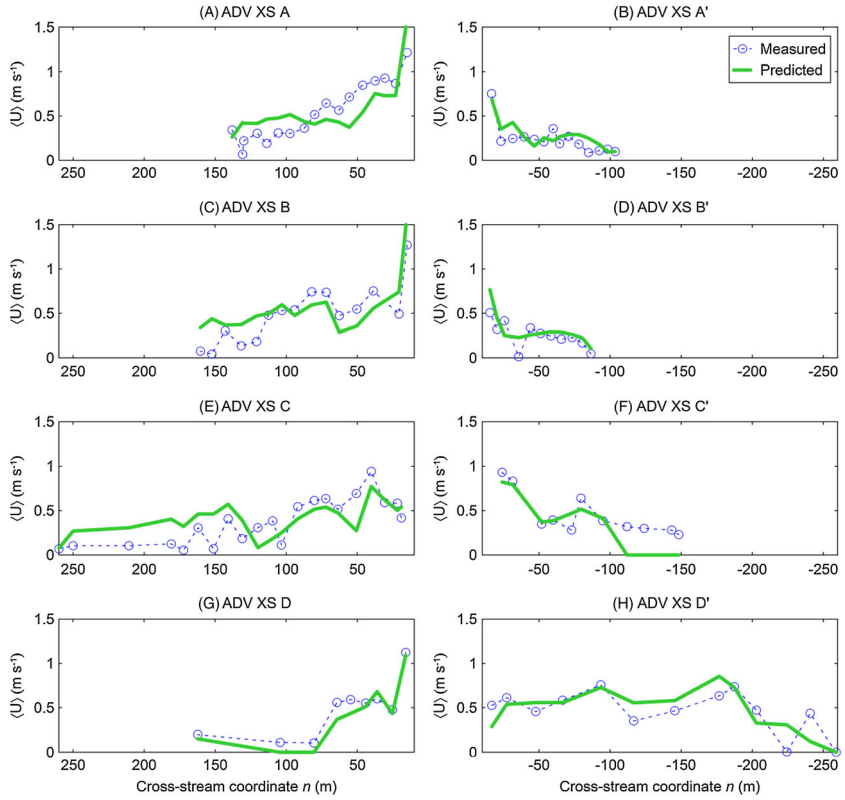

Figure 5. Comparison between measured floodplain depth-averaged velocity magnitudes with those predicted by FaSTMECH. The cross-stream coordinate $n = 0$ on the abscissa indicates the channel centerline. This figure is available in colour online at wileyonlinelibrary.com/journal/espl

The predicted bed shear stress is a function of the velocity and the drag coefficients used to represent the friction due to sediment grains and vegetation. Values of the skin drag coefficient (c_d) used in FaSTMECH have been successfully calibrated in this study and in two previous studies at this same field location (Harrison *et al.*, 2011; Legleiter *et al.*, 2011). Given the close agreement between the observed and predicted velocity magnitudes, and our confidence in the estimates of c_d, computed values of the bed shear stress due to grain friction (τ_g) along the channel bed, banks and unvegetated floodplain were assumed to provide accurate estimates of the actual stress patterns. Values of the bed shear stress in and around vegetation have not been widely measured in the field, and there is greater uncertainty in our shear stress estimates within vegetated portions of the floodplain. Direct shear stress measurements collected within floodplain vegetation remains an important research need, as highlighted recently by Vargas-Luna *et al.* (2014).

Predicted channel–floodplain flow exchange

The predicted depth, velocity and unit discharge are shown in Figure 6 for a simulated five-year flood (Q = 128.3 m^3 s^{-1}). The combination of higher channel depths and velocities, relative to the bankfull discharge, leads to greater unit discharge values in the main channel, with locally high floodplain values of unit discharge where water was expelled from the channel to the floodplain (Figure 6C).

Relatively high rates of flow exchange between the channel and floodplain were computed and measured in the zones where Wormleaton *et al.* (2004) documented the same

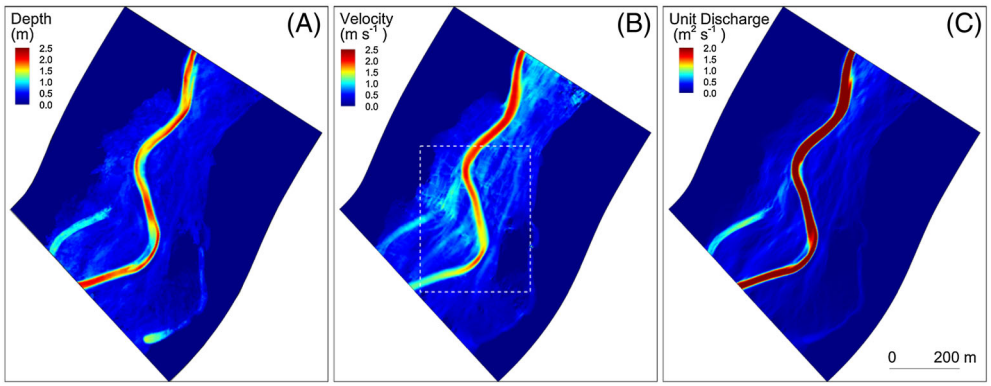

Figure 6. Simulated (A) depth, (B) velocity and (C) unit discharge for a five-year flood event. The white square in the middle panel outlines the location of the velocity contours and vectors shown in detail in Figure 7. This figure is available in colour online at wileyonlinelibrary.com/journal/espl

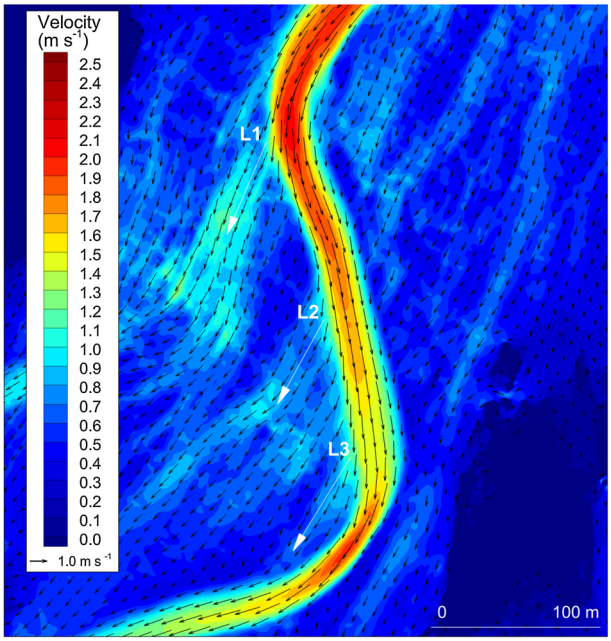

Figure 7. Flow exchange between the channel and floodplain, illustrated by the patterns of depth-averaged velocity magnitude (contours) and orientation (vectors), simulated for a five-year flood. White arrows show the locations where water was expelled from the channel to the floodplain resulting in divergent velocity vectors between the main channel and floodplain. This figure is available in colour online at wileyonlinelibrary.com/journal/espl

patterns in a laboratory flume. Concentrated zones of high-velocity water exited the channel at locations also observed by Wormleaton *et al.* (2004). Immediately downstream of the second bend apex a zone of flow ~30 m wide with a predicted velocity of 1.5 m s^{-1} leaves the outer bend of the channel and flows over a floodplain gradient of 0.0065 for 50 m (L1 in Figure 7). The downstream floodplain gradient diminishes to the reach average value (0.003) over the next 150 m, with an accompanying reduction in the predicted velocity to a value of 0.7 m s^{-1}.

A broader zone of flow leaves the right channel bank 100 m downstream of the second bend apex, with an average velocity of 0.9 m s^{-1}, and flows over an initial floodplain gradient of 0.016 for 15 m, with a lower downstream slope of 0.0024 and a mean velocity of 0.75 m s^{-1} (L2 in Figure 7). The location and width of this second outflow zone are related to the rate at which the right channel bank decreases in elevation relative to the water surface profile. In the study reach, this zone extends as far as the current point bar.

High velocity water escaped the main channel upstream from the point bar of the third bend (L3 in Figure 7), resulting in flow divergence between the high velocity core which followed the curved planform of the meander bend and water that was advected across the bar surface following the straighter path of the floodplain gradient. Water exits the channel at an average velocity of 1.25 m s^{-1} and flows over an initial gradient of 0.0046 across the upper 10 m of the point bar, then diminishes to a velocity of 0.7 m s^{-1} after flowing across the bar platform (L3 in Figure 7). The strong flow divergence at this location has led to gravel deposition > 1.5 m during three five-year flood events that have occurred since channel construction (Harrison *et al.*, 2011; Legleiter *et al.*, 2011).

The overall spatial pattern of predicted velocities was similar across flows ranging from a five-year to a 100-year flood (Figure 8). The depth, velocity and bed shear stress all increased with discharge, as a larger fraction of the total discharge was transported on the floodplain as total simulated discharge increased. The highest velocities continued to follow the main channel, and water was conveyed across the three locations shown in Figure 7, with increasing discharge.

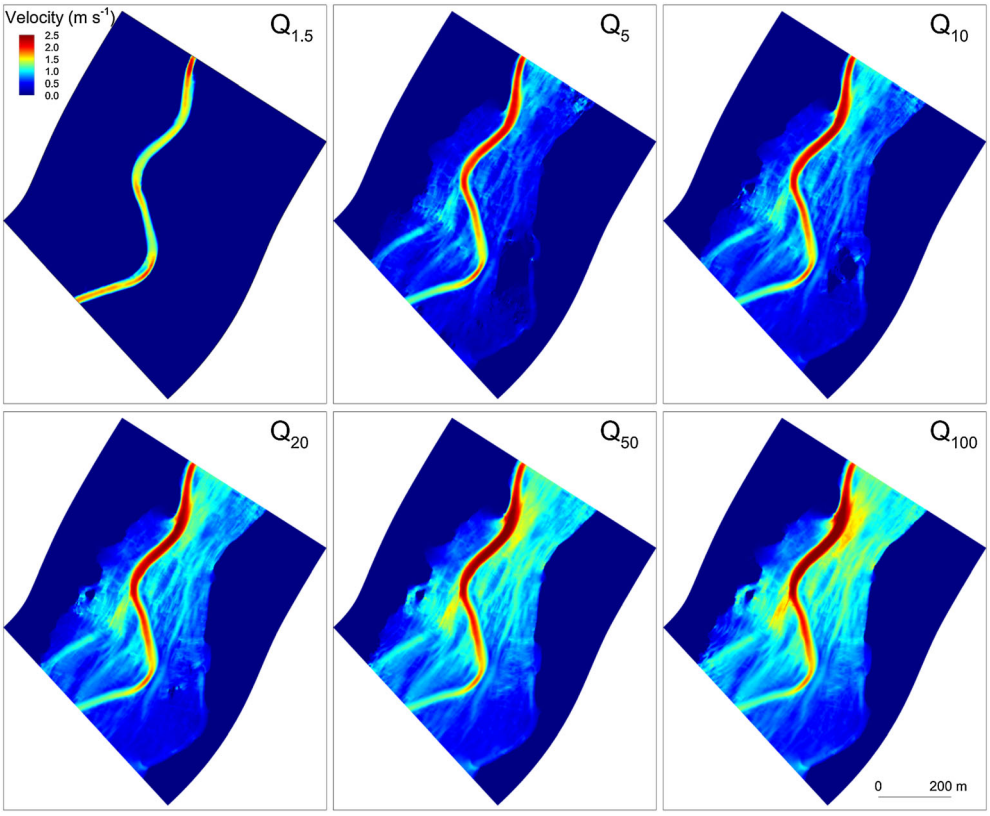

Figure 8. Simulated channel–floodplain velocity magnitudes at flows ranging between 1.5 and 100-year recurrence intervals. This figure is available in colour online at wileyonlinelibrary.com/journal/espl

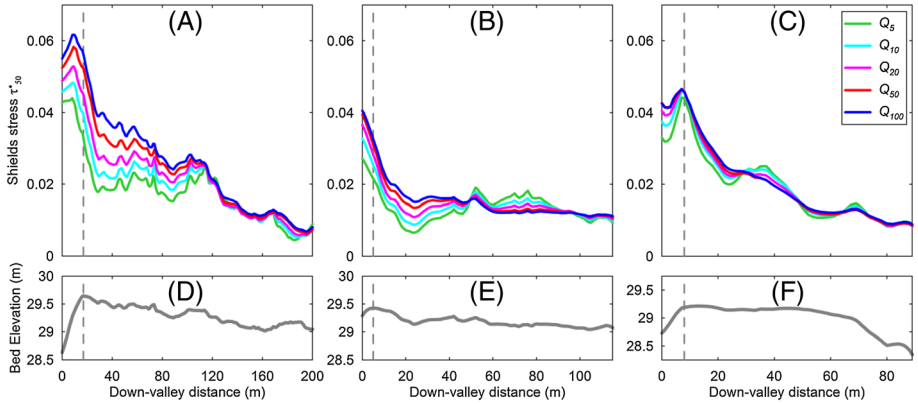

Figure 9. Variation in Shields stress along transects (A) L1; (B) L2 and (C) L3. Topographic profiles are shown below for each transect (D) L1; (E) L2 and (F) L3. Vertical dotted lines denote the channel edge. This figure is available in colour online at wileyonlinelibrary.com/journal/espl

Overbank flow and chute incision potential

The flow model results indicate three locations at which water leaves the channel with a potential to erode the floodplain surface. First, the transfer of water from the channel to the floodplain was predicted to be greatest at the second bend where the channel most strongly turned away from the down-valley direction (L1 in Figure 7). At this location water from the channel entered the floodplain and has cut a new floodplain channel that has enlarged during three overbank floods to a width of ~30 m, similar to that of the mainstem bankfull channel, and a maximum depth of 0.4 m. While the majority of the floodplain was predicted to be stable during the 5.8-year flood (mean τ^*_{50} = 0.009), local values of τ^*_{50} exceeded 0.03 at the channel–floodplain transition in this location (Figure 9A), indicating that the D_{50} (57 mm) should be at or near the threshold for sediment motion at the channel margin, while 100 m down-valley from the channel, only sizes smaller than the D_{16} (32 mm) were predicted to be mobile. Although this sediment entrainment index value does not take mixed-particle-size effects into account, it is a conservative measure of particle mobility at the site, as illustrated by particle-tagging experiments in the channel (Wydzga *et al.*, 2007). Thus, mobility was predicted even for gravel.

When compared to a 2002 DEM of the initial channel and floodplain topography (CADWR, 2005), the 2012 DEM developed in this study shows that an incipient chute has developed at this outflow location (Figures 10A and 10B), which coincides with the peak boundary shear stress prediction. Peak floodplain incision of 0.4 m at this location has eroded a well-defined, continuous floodplain channel 30 m in width, as indicated by the topographic profiles T1 and T2 in Figure 10. The development of the chute at this location (c1 in Figure 11) is favored by the position of the high velocity core, which moves from the convex bank across the channel to the outer concave bank (Figure 11B), resulting in rapid expulsion of water from the channel to the floodplain. The high velocity core moves closer to the outer bank and farther downstream with increasing discharge (Figure 11B), increasing the transfer of water from the channel to the floodplain.

A second chute, 8 m wide by 0.12 m deep, has developed along the inner bank of the third bend (L3 in Figure 7 and T3 in Figure 10). Here, the high-velocity core in the 5.8-year flood was located along the inner, convex bank (Figure 11C) due to the upstream growth of the point bar, which had also been colonized by shrubby vegetation (Figure 10 shows the extent of plant growth at T1–T4, with vegetation shown as green squares on the profiles). The vegetation was represented in our model calculations as an area of high drag coefficient (c_{dv})

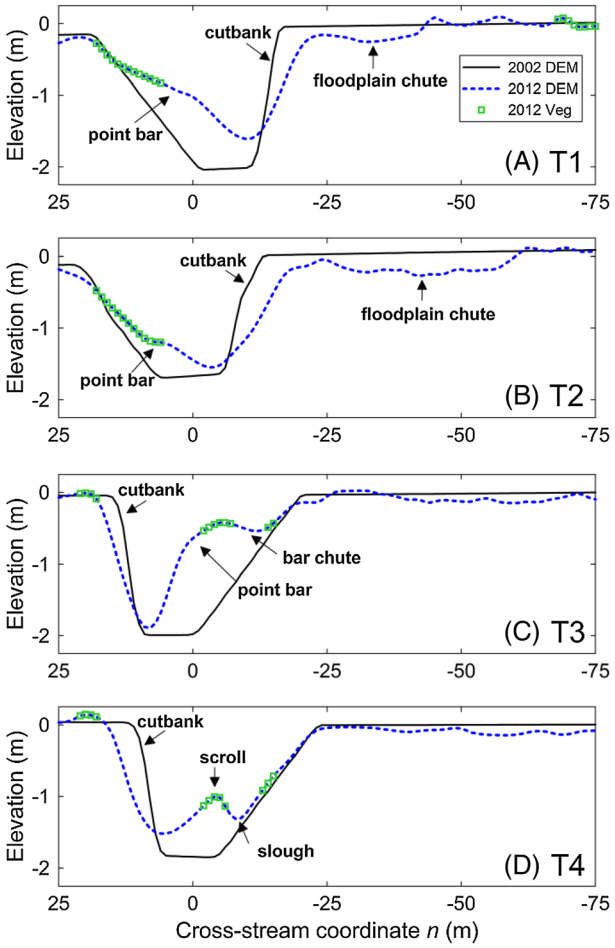

Figure 10. Topographic profiles illustrating the degree of floodplain chute formation (A, B), bar chute incision (C) and scroll-slough development (D) that have occurred since the channel was constructed in 2002. Modest incision (~0.1 m) has occurred along the right floodplain of T3 and T4 (C, D). Shrubby plants have colonized the point bars between the floodplain and low-flow stage (A, B), with gaps in the vegetation between chutes (C) and sloughs (D). Trees have also grown sporadically on the floodplain (A) and along the outer banks of meander bends (C, D). Transect locations are provided in Figure 1. The view is looking downstream. This figure is available in colour online at wileyonlinelibrary.com/journal/espl

superimposed on the topography of the bar itself, which both slows the water and deflects the high velocity core (Figure 11C), favoring deposition of bed-material load and continued bar building at the point of flow divergence. The

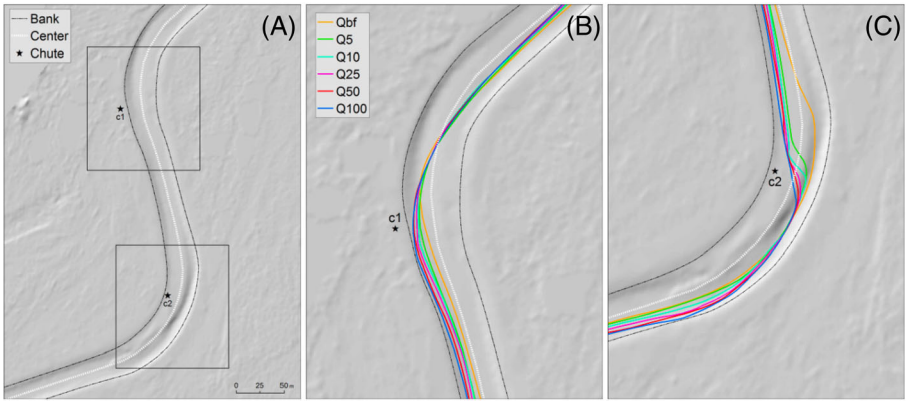

Figure 11. Predicted position of the high velocity core with increasing discharge. (A) Location of right and left banks (black lines), centerline (white line) and the entrance locations of incipient chutes (star symbols) are shown overlain on a 2012 hillshade. Modeled shifts in the high velocity core at discharges between bankfull and a 100-year flood for the second (B) and third (C) bend of the study reach. This figure is available in colour online at wileyonlinelibrary.com/journal/espl

emerging topography, the favorable gradient along the floodplain, and the resistance of the vegetation cause FaSTMECH to predict the diversion of flow inside of the bar and through the gap between the bar and the older floodplain surface. The τ^*_{50} (using a locally measured channel D_{50} = 35 mm) along this flow path in the five-year flood was 0.03–0.042 over the first 10 m of the chute (Figure 9C), predicting scouring of the gravel and the absence of settling by suspended sand (the concentration of which in the modern Merced is unnaturally low because of upstream dams).

Water also spilled from the channel to the floodplain along the right bank between the crossing and the point bar between the second and third bends (L2 in Figure 7). The magnitude and breadth of this flow are affected by the rate at which the right-bank elevation declines relative to the in-channel water surface elevation. The right bank gradient between L1 and L3 in Figure 7 was 0.004, compared to the water surface gradient of 0.002 and FaSTMECH predicted a two-fold increase in the water depth and velocity along this portion of the bank. In the case of the study reach, this bank profile is still largely the result of the construction activities. However, in natural rivers it can vary with the lateral convexity of point bar accretion, and thus with the texture and rate of growth of the point bar. In the absence of any previously developed topographic avenue, such as sloughs between scroll bars, this flow produced a τ^*_{50} between 0.01 and 0.022 (Figure 9B) in the five-year flood, predicting floodplain stability, even though the floodplain surface is bare or covered with sparse grasses. Thus flow emerging from the channel in the five-year flood was not competent to mobilize the median grain size of the floodplain sediment in this zone, although a potential would exist for incision of finer sediments in the absence of riparian vegetation. The paper by Kasvi *et al.* (2013, figure 1) illustrates (without comment) a large chute across a sandy point bar in this physiographic location.

Discussion

In-channel flow field

Our field measurements indicated that the orientation of helical flow was consistent with previous observations of in-channel flows, and we did not observe counter-acting helical flow cells reported in flume experiments conducted in two-stage channels (Sellin *et al.*, 1993; Shiono and Muto, 1998). The proposed mechanism responsible for the change in the direction of secondary flow cells in the laboratory studies is the inflow of high velocity floodplain flow to the channel at the cross-over region, which creates a circulation cell that is carried into the next downstream bend, where it acts in the opposite sense to the curvature-induced, helical flow cell (Wormleaton and Ewunetu, 2006). Development of the counter-acting flow cell is favored by unnaturally smooth floodplains and flow depths that are large relative to the bankfull depth (Sellin *et al.*, 1993). The small ratios of floodplain/channel depth (0.22) and velocity (0.3) of the study reach during the observed five-year flood lead to conditions where the channel hydraulics were not fundamentally different from the bankfull case.

Channel–floodplain interactions and chute incision potential

In this study chute formation was influenced by six factors: total discharge (with its effect on water-surface elevation), channel curvature, location of the high velocity core, floodplain gradient, erodibility of the floodplain sediment, and the flow resistance provided by vegetation. The evolving chute which is forming at the second bend (T2 in Figure 10B) has been favored by the high channel velocities along the outer bank, sparse riparian vegetation and a locally steep floodplain gradient advantage. The location of this chute is consistent with the observations of Constantine *et al.* (2010) who found that embayments formed along the outer bank in the zone of peak near-bank velocity and curvature, and in turn are extended to form floodplain chutes. The re-engineered floodplain is somewhat unique, in that the sediment particle diameter is equal to that in the channel, whereas natural floodplains in this geographic region are typically surfaced with finer sediment. If the floodplain surface were sandier, we would expect the rate of chute growth to be greater than what has been observed in the coarse material of the Merced floodplain. A sandier floodplain could also favor the occupation of the engineered floodplain channels shown in Figure 1.

The chute forming along the inner bank of the third bend (T3 in Figure 10C) has developed in part due to the inward shift of the high velocity core during overbank floods, in comparison to bankfull flows (Figure 11C). At bankfull stage, water shoals over the point bar and the high-velocity core is steered toward the outer bank (Figure 11C) by the combined effects of curvature and the bar topography, as reported in field (Dietrich *et al.*, 1979; Dietrich and Smith, 1983) and laboratory studies (Blanckaert, 2010). During overbank flows, the topographic steering effect is diminished as the bars become submerged and the high-velocity core more closely follows the channel centerline (Figure 11C), as observed in moderately curved

(Andrews and Nelson, 1989) and sharply curved meander bends (Rinaldi *et al.*, 2008). Kasvi *et al.* (2013) measured velocity transects with an ADCP along a meandering sand-bedded river at three discharges and found that the high velocity core shifted from the outer concave bank at low flow (23% of bankfull), towards the inner, convex bank at a medium (54% of bankfull) and bankfull discharges. The straightening of the high velocity core resulted in ~0.2 m of erosion at the point bar head and bar platform, while scroll bars formed on the downstream end of the point bar due to the decreased sediment transport capacity and secondary circulation cells.

The 2D flow field predicted by FaSTMECH in the Merced study for a five-year flood was similar to the bankfull discharge flow field reported by Kasvi *et al.* (2013), with an inward shift in the high velocity core across the point bar of the third bend. The inward movement of the high velocity core during overbank floods brings more sediment to the apex of the bar, which is finer than the reach-averaged D_{50}. The increased bar height and its colonization with shrubby plants increase the flow resistance and intensify the flow diversion between the main channel and the floodplain chute (L3 shown in Figure 7). The diverted flow follows a straighter path down the floodplain gradient, along which flow is competent to mobilize sediment, leaving a chute open between the vegetated portion of the point bar and the floodplain.

In our study FaSTMECH predicted a floodplain gradient advantage at each of the locations shown in Figure 7 (L1–L3). At the second bend (L1 in Figure 7) the predicted water surface gradient in the channel was 0.0033, compared to 0.0055 at the channel–floodplain margin and 0.004 along the first 30 m of the floodplain chute. The peak floodplain water surface gradient at this location is produced by super-elevation along the outer bank, which steepened the water surface slope, elevated floodplain velocities and eroded the gravelly floodplain.

Between the second and third bends (L2 in Figure 7), the water surface gradient in the channel was 0.002, compared to 0.004 on the floodplain. Here water was expelled from the channel to the floodplain along the locally steeper gradient, but the flow depth and velocity were not sufficient in the five-year flood to initiate channelized erosion. At the third bend (L3 in Figure 7), the predicted channel water surface gradient was 0.0032, compared to 0.0045 along the chute entrance. At this location, the sediment transport potential was predicted to be above the threshold for gravel entrainment, despite the absence of in-channel super-elevation, resulting in chute formation across the point bar.

Flow resistance provided by floodplain vegetation and substrate provided a fourth influence on the potential for chute formation. The absence of streamside vegetation has favored chute formation along the outer bank of the second bend and the inner bank of the third bend. The implication is that in similar geographic environments where floodplain vegetation is sparse, local accelerations and decelerations of flow caused by the curvature and alignment of the channel can affect the location of floodplain chute development. However, vegetation on the point bar can intensify the diversion of water across the bar and into the floodplain.

Results from this study highlight the fact that in the absence of dense floodplain vegetation, there appears to be an inherent tendency for meandering rivers to form chutes, an illustration of the principle proposed by Murray and Paola (1994) who developed a simple rule-based simulation of the bed-elevation changes to be expected if an initially random, wide, granular bed is subjected to flowing water. In the Merced reach, the initial channel form, riparian vegetation, a certain amount of bank-material cohesion, particle-size limitations on mobility, and the finite range of flood stage have constrained the location of chutes to two preferred locations. The long-term development of such chutes, will depend on: the erodibility of floodplain sediment, the magnitude and duration of flows out of the channel, the supply of settleable suspended sediment (Braudrick *et al.*, 2009), and the development of flow resistance by living or dead vegetation within the chute.

The potential for chute incision at a given location is sensitive to the orientation of the channel relative to the down-valley direction, which sets up the angle at which water escapes the channel onto the floodplain. Erosive overbank flow at outer-bank locations, such as the second bend, is generally favored by increasing sinuosity of the bend, growth of the opposite bar, and filling of the pool. The water flowing overbank is decanted from the upper portion of the water column and thus has low concentrations of bed material, although in the case studied here imbrication of gravel on the channel cutbank and the embayment indicated at least a small flux of bedload from the channel into the embayment. The transfer of water from the channel to the floodplain along the inner bank of the third bend initially led to bar deposition as flow divergence between the main channel and floodplain caused a reduction in sediment transport capacity and gravel deposition. The early stages of chute formation at this location thus was promoted by the depositional process of bar development, as found by Wheaton *et al.* (2013) in a study of braiding mechanisms along the gravel-bedded River Feshie, Scotland. On the Merced reach, bar development and subsequent plant colonization enhanced the flow bifurcation between the main channel and evolving chute. The episodic occurrence of the relatively large

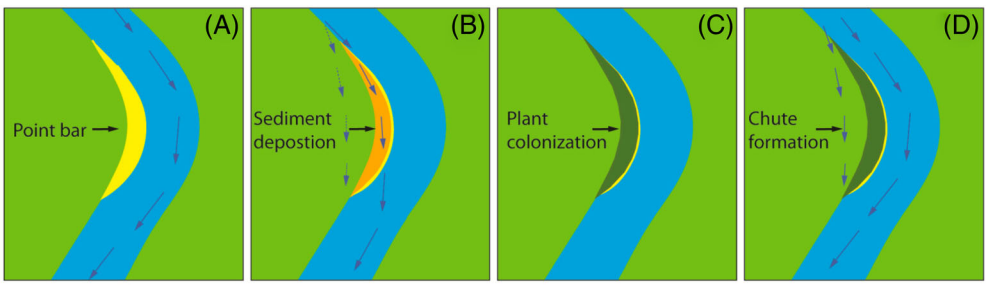

Figure 12. Conceptual model depicting initial chute formation across a point bar. (A) During bankfull flows, the high velocity core is deflected by channel curvature and the point bar (yellow) towards the cut bank, with peak velocities located downstream of the bend apex. (B) During overbank floods, flow leaves the channel (dashed blue line), water depth over the bar is greater, the high velocity core (solid blue line) shifts inward and sediment is deposited on the bar (orange). (C) Vegetation establishes on the point bar (green) while sediment is added to the top and convex margin of the bar, and the increased bar height and vegetation increase the flow resistance across the bar. (D) The zone of flow divergence between flow following the main channel and the floodplain gradient is increased due to bar development and vegetation growth, with a portion of the flow leaving the channel upstream of the point bar and resulting in chute formation. This figure is available in colour online at wileyonlinelibrary.com/journal/espl

overbank flood caused the simultaneous development of the scroll bar at some distance inboard of the previous point bar location and the scroll-slough, with the latter evolving into a chute if flow is sufficiently intense and if the entering sediment load does not force deposition. The resulting flow divergence at the point where the high-velocity core brings large sediment fluxes to the point bar intensifies the bar growth and further flow divergence into the developing chute (Figure 12). Thus, erosive overbank flow at such a location is generally favored by episodic scroll bar formation separated from the point bar, which in turn requires either relatively rapid retreat of the outer bank or the sudden inward shifting of the locus of deposition associated with the hydrodynamics of flow in the curved channel during large floods. Repetition of the scroll-slough formation process during bend extension, together with high, persistent flows and low sediment input can eventually produce chutes that are sufficiently large and favorably oriented to convey all or a significant fraction of the entire bankfull flow (Mertes *et al.*, 1996; Grenfell *et al.*, 2012).

Although we have only examined the initiation of chute formation in a single river reach with imposed channel geometry, floodplain gradient and vegetation density, we have attempted to use a combined measurement and modeling approach to analyze generalizable features of the chute formation process and to illustrate how the approach might be used for comparative studies sampling a wider range of environmental conditions.

Conclusion

Using field measurements and flow modeling, we demonstrated that secondary flow fields within meandering channels were not fundamentally different during overbank flood conditions from those observed during in-channel flows. In particular, the measurements did not confirm previous assertions that flow exchanges between channels and floodplains are strongly 3D (Wormleaton and Ewunetu, 2006). Vertical flow components did not become significantly stronger or more complex as a result of overbank flow exchanges.

Flow modeling predicted that the highest channel velocities and boundary shear stresses occurred downstream from the maxima in bend curvature even during overbank flow. This pattern was not disrupted by flows entering from the floodplain because the entrance velocity of flow from the floodplain was small in comparison with in-channel flows. Thus patterns of shear stress on the outer bank are higher and farther downstream during the five-year and larger floods than those for the bankfull flow (Figures 11B and 11C) because of the lowering of the topographic steering effect provided by the point bar. The result was the expulsion of high-velocity water with low sediment content onto the floodplain and scouring of the bank edge and floodplain surface. Topographic surveys indicate that the resulting depression is gradually extending down-valley, despite the low mobility of the gravelly floodplain. The degree to which a floodplain chute would have been deepened and extended by overbank floods on a sandier, vegetated, floodplain surface would depend on the balance of fluid forces analyzed by Constantine *et al*. (2010). The relevant result from the present measurements and modeling is to confirm the principle that the river bank immediately downstream of a bend axis, where the channel turns most abruptly from the near-bank flow trajectory and high-velocity water flows down the favorable gradient of the floodplain is one location with a relatively high potential for chute formation.

Results from the third bend also illuminate the process of chute formation across point bars, its relationship to scroll bar formation, and the eventual dominance of the scroll-slough invasion under favorable circumstances such as along large sand-bed rivers with highly erodible banks (Mertes *et al.*, 1996; Grenfell *et al.*, 2012). Alteration of upstream bend alignment or the occurrence of a large flood can shift the high-velocity core towards the center or even the inside of a bend, increasing bed material transport towards the apex of the point bar, which may emerge sufficiently to become vegetated between floods. The growing bar favors flow divergence between the two flow paths: around the curved main channel and inboard of the point bar along the floodplain gradient. If the flow and floodplain gradient are high enough and the floodplain elevation, substrate erodibility and its vegetative reinforcement low enough, shear stresses along the inboard flow path will exceed the conditions for both bedload transport and suspension. The resulting new chute will continue to focus flow along its gradient-favored path and grow to a size that is not yet predictable. As Grenfell *et al*. (2012) demonstrated, this process will be favored, and even dominated by high rates of bend extension, especially where bank erodibility is high. Other factors favoring bend extension, such as persistent, high discharge, gradient, and bend curvature will also increase the probability of flow taking the inboard route, either incising a new channel across the point bar or taking advantage of and widening scroll-sloughs.

Between the two locations described earlier, new channel formation by overbank flows is less likely because flow depths and shear stresses are lower than at locations closer to the bends. However, sufficiently high shear stresses for floodplain incision can be generated by rare large floods in these straighter reaches, especially if the vegetative cover is permanently or temporarily thin. The chute mapped, but not commented on, by Kasvi *et al*. (2013, figure 1) appears to be an example of this type. Also, as pointed out by Grenfell *et al*. (2012), scroll-sloughs, where present in this part of the floodplain are likely to be favorably aligned to capture flow if the bend has become elongated.

Acknowledgements—The research was supported by Calfed Bay-Delta Authority Science Program grant U-05SC-058, NOAA Southwest Fisheries Science Center (LRH), the Leverhulme Trust and a Visiting Professorship at the Earth Observatory of Singapore (EOS contribution 84) (TD). The authors thank Bodo Bookhagen for sharing his terrestrial LiDAR scanner. Erin Bray, Erica Meyers, Matt Meyers, Tom Snyder and Oliver Soong helped with data collection, and Carl Legleiter provided assistance in developing the kriged bed topography. A special thanks to Lynn Sullivan for piloting the jet-boat, without which the in-channel velocity measurements would not have been possible. Jose Constantine and Andrew Pike provided helpful comments on an earlier draft of the paper. The authors also thank Andrew Nicholas and an anonymous reviewer for providing reviews that greatly improved this work.

References

Andrews ED, Nelson JM. 1989. Topographic Response of a Bar in the Green River, Utah to Variation in Discharge. In *River Meandering*. American Geophysical Union: Washington, DC; 463–485.

Baptist MJ. 2005. *Modelling floodplain biogeomorphology*. Delft University of Technology: Delft; 213.

Barton GJ, McDonald RR, Nelson JM, Dinehart RL. 2005. *Simulation of Flow and Sediment Mobility using a Multidimensional Flow Model for the White Sturgeon Critical Habitat Reach, Kootenai River near Bonners Ferry, Idaho*. US Geological Survey: Reston, VA.

Bertoldi W, Tubino M. 2005. Bed and bank evolution of bifurcating channels. *Water Resources Research* **41**(7). DOI. 10.1029/2004WR003333

Blanckaert K. 2010. Topographic steering, flow recirculation, velocity redistribution, and bed topography in sharp meander bends. *Water Resources Research* **46**(9). DOI. 10.1029/2009wr008303

Blanckaert K, Graf WH. 2001. Mean flow and turbulence in open-channel bend. *Journal of Hydraulic Engineering – ASCE* **127**: 835–847. DOI. 10.1061/(asce)0733-9429(2001)127:10(835)

Braudrick CA, Dietrich WE, Leverich GT, Sklar LS. 2009. Experimental evidence for the conditions necessary to sustain meandering in coarse-bedded rivers. *Proceedings of the National Academy of Sciences of the United States of America* **106**: 16936–16941. DOI. 10.1073/pnas.0909417106

Buffington JM, Montgomery DR. 1997. A systematic analysis of eight decades of incipient motion studies, with special reference to gravel-bedded rivers. *Water Resources Research* **33**: 1993–2029. DOI. 10.1029/96WR03190

California Department of Water Resources (CADWR). 2005. *The Merced River Salmon Habitat Enhancement Project: Robinson Reach Phase III*. CADWR: San Joaquin District, Fresno, CA.

Constantine JA, McLean SR, Dunne T. 2010. A mechanism of chute cutoff along large meandering rivers with uniform floodplain topography. *Geological Society of America Bulletin* **122**: 855–869. DOI. 10.1130/b26560.1

Corenblit D, Tabacchi E, Steiger J, Gurnell AM. 2007. Reciprocal interactions and adjustments between fluvial landforms and vegetation dynamics in river corridors: a review of complementary approaches. *Earth-Science Reviews* **84**: 56–86. DOI. 10.1016/j.earscirev.2007.05.004

Crosato A, Saleh MS. 2011. Numerical study on the effects of floodplain vegetation on river planform style. *Earth Surface Processes and Landforms* **36**: 711–720. DOI. 10.1002/esp.2088

Dietrich WE, Smith JD. 1983. Influence of the point-bar on flow through curved channels. *Water Resources Research* **19**: 1173–1192. DOI. 10.1029/WR019i005p01173

Dietrich WE, Smith JD, Dunne T. 1979. Flow and sediment transport in a sand bedded meander. *Journal of Geology* **87**: 305–315.

Dunne T, Aalto RE. 2013. Large River Floodplains. In *Treatise on Geomorphology*, John FS, Wohl EE (eds). Academic Press: San Diego, CA; 645–678.

Fathi-Maghadam M, Kouwen N. 1997. Nonrigid, nonsubmerged, vegetative roughness on floodplains. *Journal of Hydraulic Engineering – ASCE* **123**: 51–57. DOI. 10.1061/(asce)0733-9429(1997)123:1(51)

Gay GR, Gay HH, Gay WH, Martinson HA, Meade RH, Moody JA. 1998. Evolution of cutoffs across meander necks in Powder River, Montana, USA. *Earth Surface Processes and Landforms* **23**: 651–662.

Grenfell M, Aalto R, Nicholas A. 2012. Chute channel dynamics in large, sand-bed meandering rivers. *Earth Surface Processes and Landforms* **37**: 315–331. DOI. 10.1002/esp.2257

Harrison LR, Legleiter CJ, Wydzga MA, Dunne T. 2011. Channel dynamics and habitat development in a meandering, gravel bed river. *Water Resources Research* **47**. DOI. 10.1029/2009wr008926

Kasvi E, Vaaja M, Alho P, Hyyppa H, Hyyppa J, Kaartinen H, Kukko A. 2013. Morphological changes on meander point bars associated with flow structure at different discharges. *Earth Surface Processes and Landforms* **38**: 577–590. DOI. 10.1002/esp.3303

Kean JW, Smith JD. 2004. Flow and boundary shear stress in channels with woody bank vegetation. In *Riparian Vegetation and Fluvial Geomorphology*. American Geophysical Union: Washington, DC; 237–252.

Knight DW, Shiono K. 1996. River channel and floodplain hydraulics. In *Floodplain Processes*, Anderson MG, Walling DE, Bates PD (eds). Wiley: New York; 139–181.

Lamb MP, Dietrich WE, Venditti JG. 2008. Is the critical Shields stress for incipient sediment motion dependent on channel-bed slope? *Journal of Geophysical Research - Earth Surface* **113**: F02008. *DOI*. 10.1029/2007jf000831

Lane SN, Bradbrook KF, Richards KS, Biron PM, Roy AG. 2000. Secondary circulation cells in river channel confluences: measurement artefacts or coherent flow structures? *Hydrological Processes* **14**: 2047–2071.

Legleiter CJ, Harrison LR, Dunne T. 2011. Effect of point bar development on the local force balance governing flow in a simple, meandering gravel bed river. *Journal of Geophysical Research* **116**. DOI. 10.1029/2010jf001838

Legleiter CJ, Kyriakidis PC. 2008. Spatial prediction of river channel topography by kriging. *Earth Surface Processes and Landforms* **33**: 841–867. DOI. 10.1002/esp.1579

Li SS, Millar RG. 2011. A two-dimensional morphodynamic model of gravel-bed river with floodplain vegetation. *Earth Surface Processes and Landforms* **36**: 190–202. DOI. 10.1002/esp.2033

Lisle TE, Nelson JM, Pitlick J, Madej MA, Barkett BL. 2000. Variability of bed mobility in natural, gravel-bed channels and adjustments to sediment load at local and reach scales. *Water Resources Research* **36**: 3743–3755. DOI. 10.1029/2000WR900238

Markham AJ, Thorne CR. 1992. Geomorphology of gravel-bed river bends. In *Dynamics of Gravel-bed Rivers*, Billi P, Hey RD, Thorne CR, Taconni P (eds). John Wiley & Sons: Chichester; 433–456.

McDonald RR, Nelson JM, Bennett JP. 2005. *Multidimensional Surface-water Modeling System User's Guide*, USGS Techniques in Water Resources Investigations 11-B2. US Geological Survey: Reston, VA; 156.

McGowen JH, Garner LE. 1970. Physiographic features and stratification types of coarse-grained point bars – modern and ancient examples. *Sedimentology* **14**: 77–111. DOI. 10.1111/j.1365-3091.1970.tb00184.x

Mertes LAK, Dunne T, Martinelli LA. 1996. Channel–floodplain geomorphology along the Solimoes-Amazon River, Brazil. *Geological Society of America Bulletin* **108**: 1089–1107.

Morvan H, Pender G, Wright NG, Ervine DA. 2002. Three-dimensional hydrodynamics of meandering compound channels. *Journal of Hydraulic Engineering – ASCE* **128**: 674–682. DOI. 10.1061/(Asce)0733-9429(2002)128:7(674)

Murray AB, Paola C. 1994. A cellular-model of braided rivers. *Nature* **371**: 54–57. DOI. 10.1038/371054a0

Nelson JM, Bennett JP, Wiele SM. 2003. Flow and sediment transport modeling. In *Tools in Fluvial Geomorphology*, Kondolf GM, Piegay H (eds). John Wiley & Sons: Chichester; 539–576.

Nepf HM. 2012. Hydrodynamics of vegetated channels. *Journal of Hydraulic Research* **50**: 262–279. DOI. 10.1080/00221686.2012.696559

Nicholas A. 2013. Morphodynamic diversity of the world's largest rivers. *Geology* **41**: 475–478. DOI. 10.1130/G34016.1

Nicholas AP, McLelland SJ. 2004. Computational fluid dynamics modelling of three-dimensional processes on natural river floodplains. *Journal of Hydraulic Research* **42**: 131–143. DOI. 10.1080/00221686.2004.9628299

Nicholas AP, Mitchell CA. 2003. Numerical simulation of overbank processes in topographically complex floodplain environments. *Hydrological Processes* **17**: 727–746. DOI. 10.1002/hyp.1162

Parsons DR, Jackson PR, Czuba JA, Engel FL, Rhoads BL, Oberg KA, Best JL, Mueller DS, Johnson KK, Riley JD. 2013. Velocity Mapping Toolbox (VMT): a processing and visualization suite for moving-vessel ADCP measurements. *Earth Surface Processes and Landforms* **38**(11): 1244–1260. DOI. 10.1002/esp.3367

Perroy RL, Bookhagen B, Asner GP, Chadwick OA. 2010. Comparison of gully erosion estimates using airborne and ground-based LiDAR on Santa Cruz Island, California. *Geomorphology* **118**: 288–300. DOI. 10.1016/j.geomorph.2010.01.009

Rinaldi M, Mengoni B, Luppi L, Darby SE, Mosselman E. 2008. Numerical simulation of hydrodynamics and bank erosion in a river bend. *Water Resources Research* **44**. DOI. 10.1029/2008wr007008

Sellin RHJ, Ervine DA, Willetts BB. 1993. Behavior of meandering 2-stage channels. *Proceedings of the Institution of Civil Engineers – Water Maritime and Energy* **101**: 99–111.

Shiono K, Muto Y. 1998. Complex flow mechanisms in compound meandering channels with overbank flow. *Journal of Fluid Mechanics* **376**: 221–261. DOI. 10.1017/s0022112098002869

Smith JD. 2004. The role of riparian shrubs in preventing floodplain unraveling along the Clark Fork of the Columbia River in the Deer Lodge Valley, Montana. In *Riparian Vegetation and Fluvial Geomorphology*. American Geophysical Union: Washington, DC; 71–85.

Stoesser T, Wilson CAME, Bates PD, Dittrich A. 2003. Application of a 3D numerical model to a river with vegetated floodplains. *Journal of Hydroinformatics* **5**: 99–112.

Takebayashi H, Okabe T. 2009. Numerical modelling of braided streams in unsteady flow. *Proceedings of the Institution of Civil*

Engineers – Water Management **162**: 189–198. DOI. 10.1680/wama.2009.00011

Tal M, Paola C. 2007. Dynamic single-thread channels maintained by the interaction of flow and vegetation. *Geology* **35**: 347–350. DOI. 10.1130/g23260a.1

Termini D, Piraino M. 2011. Experimental analysis of cross-sectional flow motion in a large amplitude meandering bend. *Earth Surface Processes and Landforms* **36**: 244–256. DOI. 10.1002/esp.2095

Vargas-Luna A, Crosato A, Uijttewaal WSJ. 2014. Effects of vegetation on flow and sediment transport: comparative analyses and validation of predicting models. *Earth Surface Processes and Landforms* **40**(2): 157–176. DOI. 10.1002/esp.3633

Wheaton JM, Brasington J, Darby SE, Kasprak A, Sear D, Vericat D. 2013. Morphodynamic signatures of braiding mechanisms as expressed through change in sediment storage in a gravel-bed river. *Journal of Geophysical Research - Earth Surface* **118**(2): 759–779. DOI. 10.1002/jgrf.20060

Wiberg PL, Smith JD. 1987. Calculations of the critical shear stress for motion of uniform and heterogeneous sediments. *Water Resources Research* **23**: 1471–1480. DOI. 10.1029/WR023i008p01471

Wilson C, Horritt MS. 2002. Measuring the flow resistance of submerged grass. *Hydrological Processes* **16**: 2589–2598. DOI. 10.1002/hyp.1049

Wormleaton PR. 1996. Floodplain secondary circulation as a mechanism for flow and shear stress redistribution in straight compound channels. In *Coherent Flow Structures in Open Channels*, Ashworth PJ, Bennett SJ, Best JL, McClelland SJ (eds). John Wiley & Sons: Chichester; 581–608.

Wormleaton PR, Ewunetu M. 2006. Three-dimensional k–∈ numerical modelling of overbank flow in a mobile bed meandering channel with floodplains of different depth, roughness and planform. *Journal of Hydraulic Research* **44**: 18–32. DOI. 10.1080/00221686.2006.9521658

Wormleaton PR, Sellin RHJ, Bryant T, Loveless JH, Hey RD, Catmur SE. 2004. Flow structures in a two-stage channel with a mobile bed. *Journal of Hydraulic Research* **42**: 145–162. DOI. 10.1080/00221686.2004.9628300

Wydzga MA, Legleiter CJ, Dunne T. 2007. Predicting bed mobility in a simple river channel. *Proceedings, American Geophysical Union, Fall Meeting*, San Francisco, CA.